

Influence of Coronal Holes on CMEs in Causing SEP Events

Chenglong Shen^{1,2}, Jia Yao¹, Yuming Wang¹, Pinzhong Ye¹, X. P. Zhao³ and S. Wang¹

¹ CAS Key Laboratory of Basic Plasma Physics, School of Earth & Space Sciences, University of Science & Technology of China, Hefei, Anhui 230026, People's Republic of China
(clshen@ustc.edu.cn, ymwang@ustc.edu.cn)

² State Key Laboratory of Space Weather, Chinese Academy of Science, Beijing, 100080, China.

³ W. W. Hansen Experimental Physics Laboratory, Stanford University, Stanford, CA 94305.

Abstract The issue of the influence of coronal holes (CHs) on coronal mass ejections (CMEs) in causing solar energetic particle (SEP) events is revisited. It is a continuation and extension of our previous work (Shen et al., 2006), in which no evident effect of CHs on CMEs in generating SEPs were found by statistically investigating 56 CME events. This result is consistent with the conclusion obtained by Kahler in 2004. In this paper, we extrapolate the coronal magnetic field, define CHs as the regions consisting of only open magnetic field lines and perform a similar analysis on this issue for totally 76 events by extending the study interval to the end of 2008. Three key parameters, CH proximity, CH area and CH relative position, are involved in the analysis. The new result confirms the previous conclusion that CHs did not show any evident effect on CMEs in causing SEP events.

Key words: acceleration of particles — Sun: coronal mass ejections — Sun: coronal holes — Sun: particle emission

1 INTRODUCTION

Gradual solar energetic particle (SEP) events are thought to be a consequence of CME-driven shocks generating plenty of SEPs which would be observed near the Earth. In our previous work in 2006, we statistically studied the effect of coronal holes (CHs) on the CMEs causing SEP events by investigating the CME source locations and their relation with the CHs identified in EUV 284 Å (Shen et al., 2006, hereafter Paper I). It was implied that neither CH proximity nor CH relative location exhibits any evident effect on the intensities of SEP events. This result is consistent with the conclusion obtained by Kahler (2004), who comparatively studied the SEP events produced in the fast and slow solar wind streams and found no significant bias against SEP production in fast-wind regions which are believed to originate from CHs.

These findings seem not quite fit people's 'common sense', because CHs are believed to be regions with low-density and low temperature in the corona (e.g. Harvey & Recely, 2002), from which the solar wind is fast and the magnetic field is open, and therefor apparently three disadvantages for a CME to produce SEP may exist when it is near a coronal hole region. These advantages are: (1) the background solar wind speed V_{sw} near CHs is larger than that in other regions; (2) the plasma density near CHs is much lower than that in other regions, so that the Alfvén speed V_a is larger (Shen et al., 2007; Gopalswamy et al., 2008); and (3) the magnetic field lines in CHs are open. The first two disadvantages

suggest that a strong shock might be hardly produced near CHs. The third one implies that particles might be able to escape from the shock acceleration process earlier and easier. Thus, it can be expected that CHs would influence the CME in producing SEP events. The work by Kunches & Zwickl (1999) was consistent with the picture depicted above. In their paper, they found that the CH may delay the onset times of SEPs when a CH is present between Sun-observer line and the solar source of the SEP event. They also speculate that the peak intensity could be influenced by CH. However, they did not statistical study such influence. It is hard to say that their conclusion is statistically significant.

In principle, CHs are open field regions, though they were first identified in observations (e.g. Zirker, 1977). Kunches & Zwickl (1999) identified CHs based on He 10830 Å. In our 2006 work (Paper I), CHs were auto-determined based on EUV 284Å images taken by SOHO/EIT. Thus, it is doubtful whether or not the CHs identified in EUV wavelengths really represent open field regions. Another doubt in our 2006 work is that only frontside CHs are taken into account. In order to remove the doubt and get a more reliable result, we look into this topic again by extrapolating coronal magnetic field instead of analyzing EUV images. The term ‘CHs’ in this paper therefore actually refers to open field regions. The magnetic field extrapolation and determination of CHs are introduced in Section 2. Section 3 presents the statistical analysis. A brief summary and conclusions are given in Section 4.

2 DETERMINATION OF CORONAL HOLES

So far, there are no observations of coronal magnetic field. Most information of coronal magnetic field comes from various extrapolation techniques (e.g. Schatten et al., 1969; Altschuler & Newkirk, 1969; Schatten, 1971; Zhao & Hoeksema, 1992, 1994, 1995; Zhao et al., 2002). In this paper, the current sheet-surface source (CSSS) model developed by Zhao and his colleagues (Zhao & Hoeksema, 1995; Zhao et al., 2002) will be used to extrapolate the coronal magnetic field and identify the coronal hole regions. In our calculation, the daily-updated synoptic charts of photospheric magnetic field from the Michelson Doppler Imager (MDI (Scherrer et al., 1995)) on board SOHO spacecraft is adopted as the bottom boundary condition, the extrapolated global magnetic field is a kind of average over the Carrington rotation, and may not exactly reflect the state at the time of interest. However, because CHs are long-lived structures in the solar atmosphere, we think that such approximation of global field would not significantly distort our results. To determine where are open field regions, we design 180-by-90 grid points (a point every 2 degree in longitude and 1/45 in sine latitude) at photosphere as the roots of magnetic field lines. In other words, a total of 16200 field lines will be traced to check if they are open or closed.

By using this method, CHs are defined as the regions consisting of open magnetic field lines on the photosphere. Neighboring regions with a spherical separate distance $\leq 7.5^\circ$ are grouped as one region. Those small regions with area less than $0.0024 A_s$ were discarded to raise the credibility of the determined CHs. Here A_s is the total area of solar surface. The size of $0.0024 A_s$ is about a $10^\circ \times 10^\circ$ grid at the center of the solar disk (the projection of the Sun on the plane of sky). The projection effect has been corrected in the calculation of the area of open magnetic field regions. Compared with the previous approach developed by Shen et al. (2006), this method can not only obtain all CHs over the full solar surface (not just those on the front-side solar disk), but also dig out the CHs covered by some bright structures (e.g., active regions) in EIT 284 Å images.

Figure 1 shows an example on 2000 September 16, which was also presented in Paper I. The asterisks in Figure 1(a) denote the open field regions inferred by the method (the Carrington map has been re-mapped on the solar sphere). Figure 1(b) and Figure 1(c) show the corresponding EIT 284Å image over-plotted with the CH boundaries determined in Paper I and Kitt Peak CH map for comparison.

It is obvious that CHs obtained here are similar to, but not the same, as those in the other two. The CHs presented in the EIT 284Å is in high corona and the Kitt Peak CHs is in lower corona (Harvey & Recely, 2002), whereas our extrapolated CHs is on the photosphere. As CHs may expand rapidly and superradially with increasing height (Munro & Jackson, 1977; Fisher & Guhathakurta, 1995; DeForest et al., 2001), the difference in altitude between them probably is one of the major causes of the apparent difference in the CH shape. The regions determined here could be treated as the roots

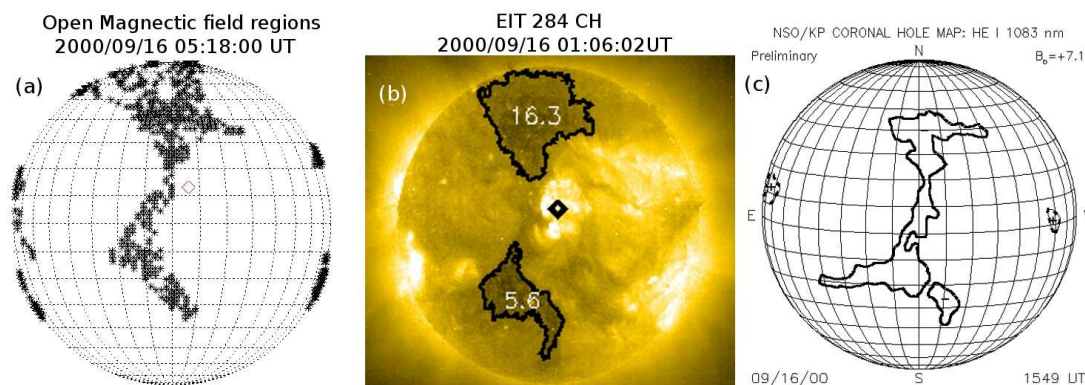


Fig. 1 (a) An example on 2000 September 16 showing CH determination by our method, the regions marked by crosses are the determined CHs, and the diamond indicates the CME location. (b) The corresponding EIT 284Å image superimposed with CH boundaries obtained by the method in Paper I, (c) Kitt Peak CH map.

of CHs. Besides, the CHs at east and west limbs in Figure 1(a) and Figure 1(c) can not be recognized in Figure 1(b). This is because of the shielding of the brightness of nearby active region. In addition, the same CH also exhibit different shapes and properties at different panels. The big CH extended from north to south in center longitude region shown in Figure 1(a) and Figure 1(c) has been divided into two separated CHs in Figure 1(b). This may also because that the brightness of the active region shield the dark region located at solar center, which makes this big CH seems like two isolated dark region.

3 STATISTICAL RESULTS

In this paper, the time period of 1997 – 2003 we used in paper I is extended to the end of 2008. All fast halo CME events originating from west hemisphere during this period are studied. As the same as we did in Paper I, the ‘fast’ and ‘halo’ mean that the CME projected speed measured in SOHO/LASCO is larger than 1000 km/s and the span angle is larger than 130° . Since the daily-updated magnetic field synoptic chart on 1998 November 5 is not available for use, the event occurred on that day is excluded. Thus a total of 76 events will be analyzed. Table 1 lists the events including the parameters of CMEs, CHs and SEPs. The key parameters we used to analyze the effect of CHs on CMEs in producing SEPs are the CH proximity (column 6), the area of the CH nearest to the CME (column 7) and the relative position of the CH (column 8). All parameter have the same meaning as those in Paper I.

It should be noted that the parameters of CHs we obtained in this paper were differ from Paper I, which may be caused by the following reasons:

1. The nearest CHs for large number of events were changed:
 - (a) As shown in Figure 1, the dark regions of CHs shielded by the brightness of active region in EIT 284Å images can be obtained in this paper. This makes the nearest CHs change in 26 events.
 - (b) CHs located in solar limb and backside has also been taken into account in this paper as we discussed in Section 2. In this paper, the nearest CHs changed to the limb or backside CHs in totally 14 events.
2. For other 15 events, same CHs in this paper and paper I were used. It is found that the areas of these 15 CHs were smaller than we obtained in paper I. In this paper, the CH we obtained can be treated as the roots of CHs. As CHs may expand rapidly and superradially with increasing height (Munro & Jackson, 1977; Fisher & Guhathakurta, 1995; DeForest et al., 2001), such result could be expected.

Such variations make the properties of nearest CHs changed largely. As we discussed before, the nearest CHs in totally 40 events changed. Even for same CH, the difference CH shape and different CH height also makes the properties of near CHs change. In this paper, the relative position of 26 events changed, and 20 events in which were changed from ‘N’ to ‘Y’. Because of variation of the nearest CHs and the height and shape of same CHs, the group of CH area and CH proximity would hard to be compared.

For simplicity and reliability, we binarize the key parameters before further analysis. The events with CH proximity larger than $0.31 R_s$ are marked as ‘D’ and the others marked as ‘d’. The events with the CH area larger/smaller than $0.0061 A_s$ are marked as ‘A’/‘a’. The parameter of the CH relative position is already bi-valued. The separation values $0.31 R_s$ and $0.0061 A_s$ are chosen to make the events near-equally divided into two groups for the CH proximity and area, respectively. In the following subsections, we will present the analysis on these difference parameters.

3.1 The dependence of CH proximity

Figure 2 shows the occurrence probabilities, P , of SEP events in terms of the CH proximity for proton energies ≥ 10 MeV (Panel a) and ≥ 50 MeV (Panel b). The SEP events at difference flux levels are presented by difference bins. For the SEP event with proton energy ≥ 10 MeV, the three levels are all SEP events, SEP events with proton flux ≥ 10 pfu and ≥ 100 pfu, in which $1 \text{ pfu} = 1 \text{ particle cm}^{-2} \text{ s}^{-1} \text{ sr}^{-1}$. For the SEP event with proton energy ≥ 50 MeV, they are all SEP events, SEP events with proton flux ≥ 1 pfu and ≥ 10 pfu. Different lines show the probabilities at different groups. The probabilities at group ‘d’ and ‘D’ are indicated by solid and dashed lines with error bars, respectively. The CME number in each group is marked in the bracket at the top right of the figure. The error bars indicate the one standard deviation (σ) level, which is given by $\sigma = \sqrt{P(1-P)/N}$, where N is the total number of CME events for the corresponding bin.

It is found that the difference of occurrence probabilities of SEP events between these two groups are small for all flux and energy levels. All differences between these two groups are less than the value of one standard deviation (1σ). Such analysis confirm the result we obtained in paper I that CHs proximity have no evident effect on CMEs in producing SEP events.

Further, the correlation between the peak intensities of SEP events and the speed of associated CMEs is studied (shown in Figure 3). Asterisks in Figure 3 show the events in group ‘d’ and diamonds show the events in group ‘D’. Points at peak intensity of 0.01 means no SEP event associated (called as SEPNCMEs in short). Panel (a) and Panel (b) in this figure shows the events with proton energy ≥ 10 MeV and ≥ 50 MeV, respectively. From this figure, it is found that the SEP associated CMEs (called as SEPYCMEs in short) were faster than SEPNCMEs. Almost all (15/16) extremely fast CMEs with speed $\geq 2000 \text{ km/s}$ were associated with SEP events.

Table 2 gives the comparison of the speed of CMEs at different groups. Difference columns show the mean value of CME speed at different groups binarized by CH proximity, CH area and relative position respectively. The first and second rows show the value of SEPYCMEs and SEPNCMEs for the SEP event with proton energy ≥ 10 MeV, while the third and fourth rows show them for proton energy ≥ 50 MeV respectively.

Third and fourth columns of Table 2 shows the comparison of CME speed at different groups binarized by CH proximity (group ‘d’ and ‘D’). It is found that the speed of SEPYCMEs in group ‘d’ and ‘D’ are almost the same. Meanwhile, the speed of SEPNCMEs in these two groups are also similar. Such results imply that no significant fast CMEs were required for producing SEP events when CMEs close to CHs. This result is consistent with Kahler (2004)’s result that no significant fast CME were required for producing the SEP events in fast solar wind region.

3.2 The dependence of CH area

Figure 4 shows the occurrence probabilities, P , of SEP events in terms of the closest-CH area for proton energies ≥ 10 MeV and ≥ 50 MeV. For the SEP events with proton energies ≥ 10 MeV shown as Figure 4(a), the occurrence probabilities of SEP events in group ‘A’ are smaller than them in group ‘a’ at large

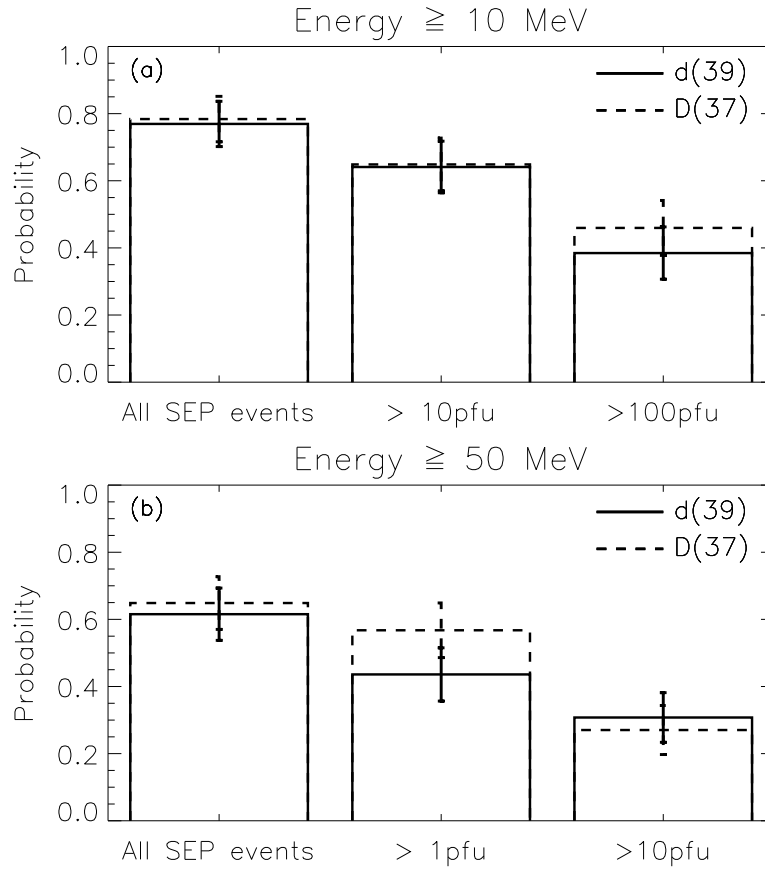


Fig. 2 Occurrence probabilities, P , of SEP events in terms of the CH proximity for proton energies ≥ 10 MeV and ≥ 50 MeV, respectively. The probabilities at different groups are indicated by solid and dashed lines with error bars, respectively. Difference bins show the probabilities at different flux levels. For the SEP at energies ≥ 10 MeV, three levels are all SEP events, ≥ 10 and ≥ 100 pfu events, in which 1 pfu = 1 particle $\text{cm}^{-2} \text{s}^{-1} \text{sr}^{-1}$. For the SEP at energies ≥ 50 MeV, they are all SEP events, ≥ 1 and ≥ 10 pfu events.

flux levels (≥ 10 pfu and ≥ 100 pfu). But, such difference between them are very small. For the SEP events with proton energy ≥ 50 MeV (Figure 4(b)), the occurrence probabilities of SEP events in group 'A' are all smaller than them in group 'a'. The difference between group 'a' and 'A' for the SEP events with proton energy ≥ 50 MeV are bigger than them for the SEP events with proton energy ≥ 10 MeV and became larger with the increasing of the flux level. Even so, such difference are still small and less than 1σ . Thus, the areas of corresponding CHs did not show any evident influence on the CME in generating SEPs.

The peak intensity varied with the associated CME speed for group 'a' and 'A' are shown in Figure 5 while the mean value of the speed of SEPYCMEs and SEPNCMEs are also listed in Table 2 (5th and 6th column). Similar with the analysis of CH proximity, no obvious difference of CME speed distribution between group 'a' and 'A' could be found. The mean value of the speed of SEPYCMEs and SEPNCMEs in these two groups are also similar. This result confirms that the area of corresponding CHs show no evident influence on CME in producing SEP event.

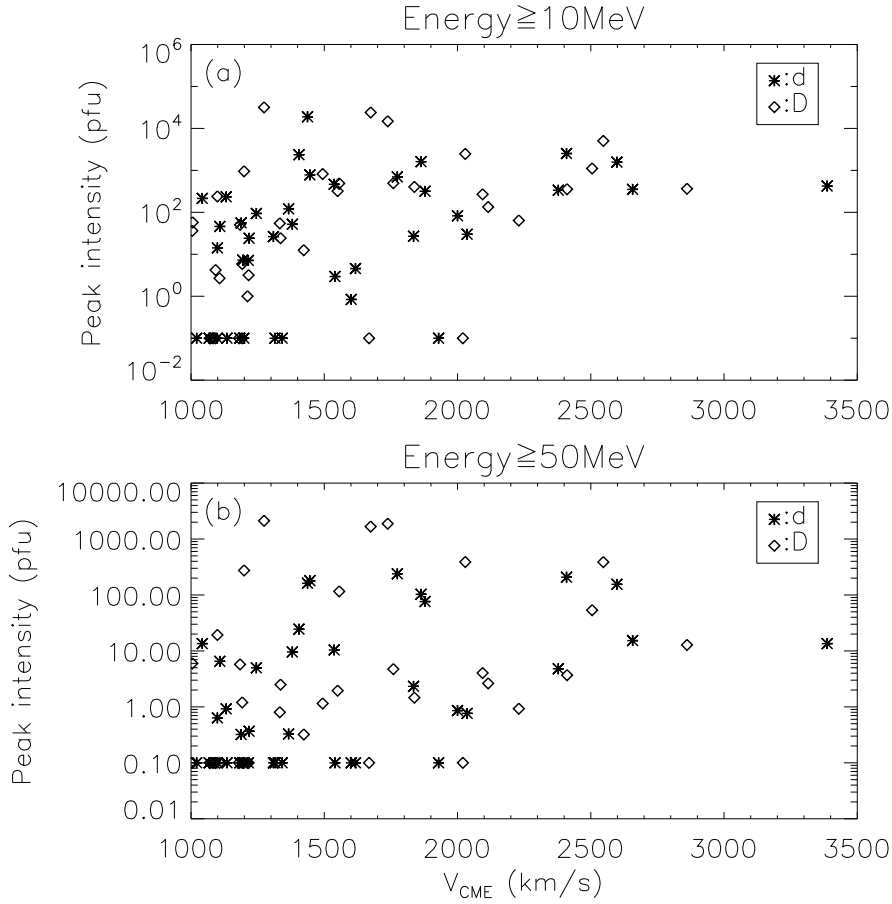


Fig. 3 The peak intensity of proton with energy ≥ 10 MeV vs. associated CME speed for proton energy ≥ 10 MeV (Panel a) and ≥ 50 MeV (Panel b). The asterisks show the CME events in group ‘d’ while diamonds show the CME events in group ‘D’. Points at peak intensity of 0.01 means no SEP associated.

3.3 The dependence of relative position

Further, the possible impact of CHs location relative to the corresponding CMEs is studied. Figure 6 shows the SEP occurrence probability of CMEs at different flux levels and different energy levels. It is found that the SEP occurrence probability of CMEs at all flux levels and energy levels in group ‘Y’ are smaller than them in group ‘N’. Specially, for the SEP events with flux level ≥ 10 pfu with proton energy ≥ 10 MeV, the SEP occurrence in group ‘Y’ is much small than it in group ‘N’. The difference between these two groups is larger than 1σ at this level. But, such difference between these two groups are small and less than the value of 1σ for all the other levels. The comparison of the speed of SEPYCMEs for group ‘Y’ and ‘N’ is shown in Figure 7. As similar as we gotten in the analysis of CH proximity and CH area, no obvious difference of the speed of SEPYCMEs between group ‘Y’ and ‘N’ could be found. The average speed of SEPYCMEs is similar as the average speed of SEPNCMEs as listed in last two columns of Table 2. These results imply that the relative location of CHs to the corresponding CMEs has no evident effect on SEP events as the same as we get in Paper I.

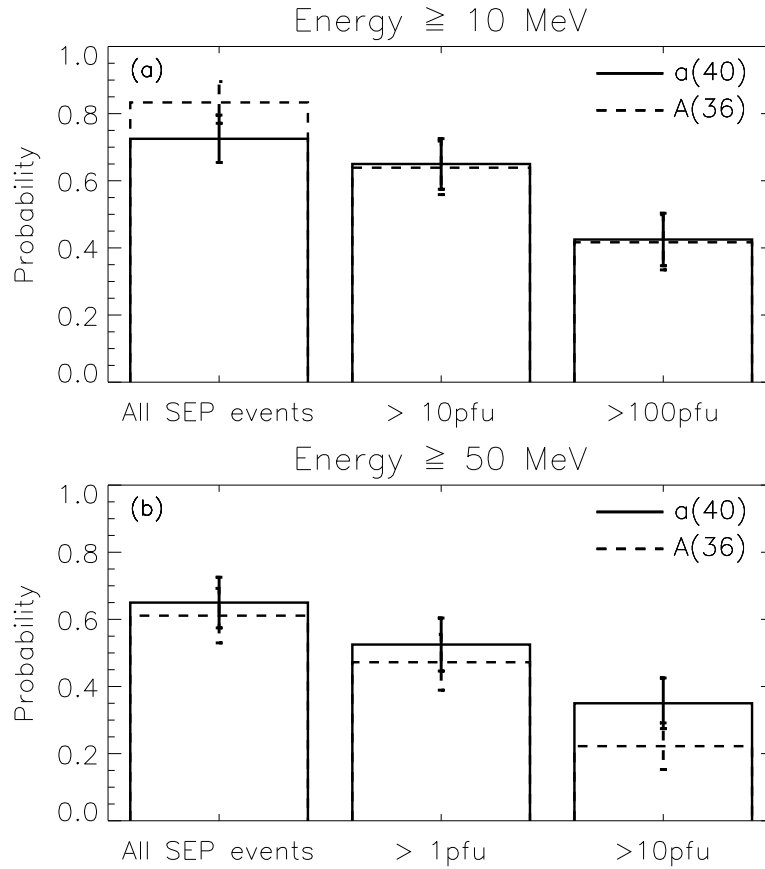


Fig. 4 Occurrence probabilities, P , of SEP events in terms of CH area for proton energies ≥ 10 MeV and ≥ 50 MeV, respectively.

4 SUMMARY AND CONCLUSIONS

In order to study the influence of CHs on CMEs in producing SEP events, a total of 76 west-side fast halo CMEs during 1997 - 2008 are investigated, as well as their associated CHs. Different from the CHs obtained by brightness method based on EIT 284Å data in paper I, the CHs we investigated in this paper are obtained with the aid of the extrapolation of coronal magnetic field by CSSS model, in which the MDI daily-updated synoptic magnetic field charts are adopted as the bottom boundary condition. By using this method, all the CHs, defined as the regions consisting of open magnetic field lines only, over the entire solar surface are inferred.

After analyzing three parameters, CH proximity, area of corresponding CHs and relative position between CHs and CMEs, it is found that all of the statistical results do NOT have significance exceeding the 1σ level. These parameters do NOT show any evident influence on SEP occurrence probability, and the speed of SEP/CMEs also do NOT show any difference between different groups binarized by these parameters. These results confirmed the conclusion we got in Paper I and Kahler (2004) that no evident influence of CHs on CME in producing SEP events.

An expanding CME may drive a quasi-parallel shock at its flank as discussed by Kahler (2004). The condition of CME in driven shock in this situation is V_{cme} larger than local alfvén speed V_a or

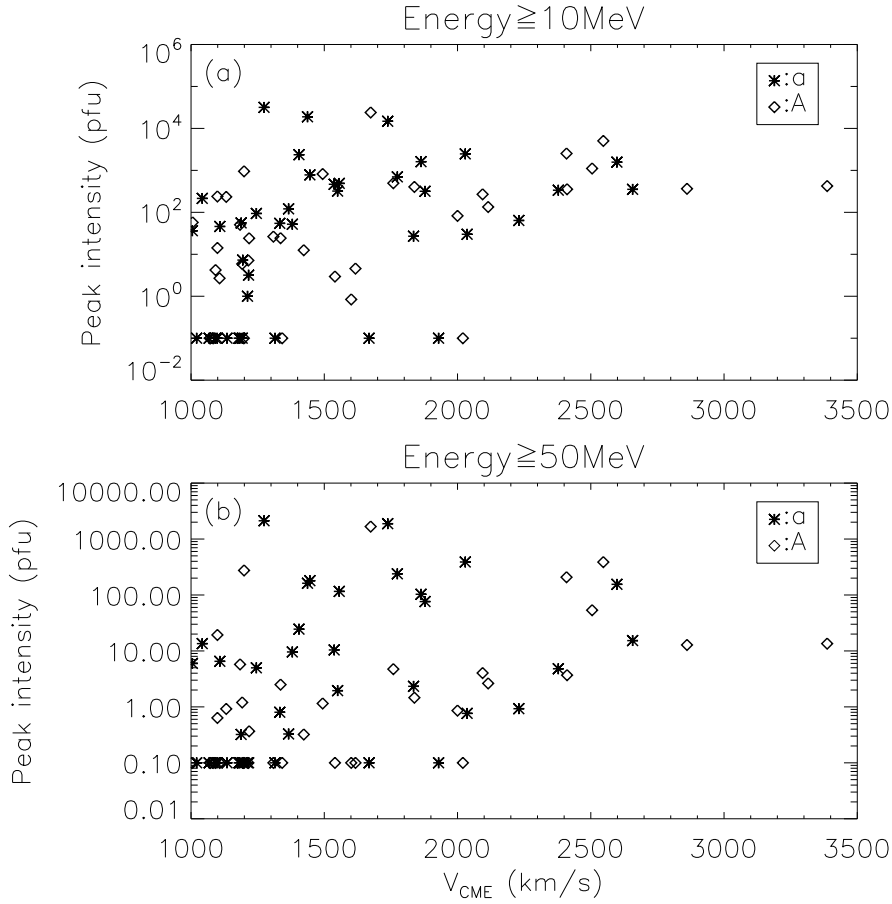


Fig. 5 The peak intensity of proton with energy ≥ 10 MeV vs. associated CME speed. The asterisks show the CMEs in group 'a' while diamonds show the CME in group 'A'.

sound speed C_s only. Thus, the fast flow speed near CHs may show no influence on producing strong shock. Beside, not only the plasma density but also the magnetic field strength in fast solar wind region is smaller than them in slow solar wind region (Ebert et al., 2009), so the alfvén speed in fast solar wind region may not be obvious faster than it in slow solar wind region. Based on these analyses, it could be expected that shock can also be produced in fast solar wind region near CH and no evident fast CME is needed. In addition, the shock interacting with background solar wind may generate turbulence. Such turbulence could be treated as the main mechanism that makes particles back to shock acceleration process to produce SEP events (Reames, 1999). The close magnetic topology could only provide an additional method to make the particle back to shock acceleration (Shen et al., 2008). So, the influence of open magnetic field topology may be weak in shock-producing SEP events.

Acknowledgements We acknowledge the use of the data from the SOHO, Yohkoh and GOES spacecraft, the CH maps from the Kitt Peak Observatory. SOHO is a project of international cooperation between ESA and NASA. This work is supported by grants from the National Natural Science Foundation of China (40904046, 40874075, 40525014), the 973 National Basic Research Program (2006CB806304), Ministry of Education of China (200530), the Program for New Century Excellent Talents in University

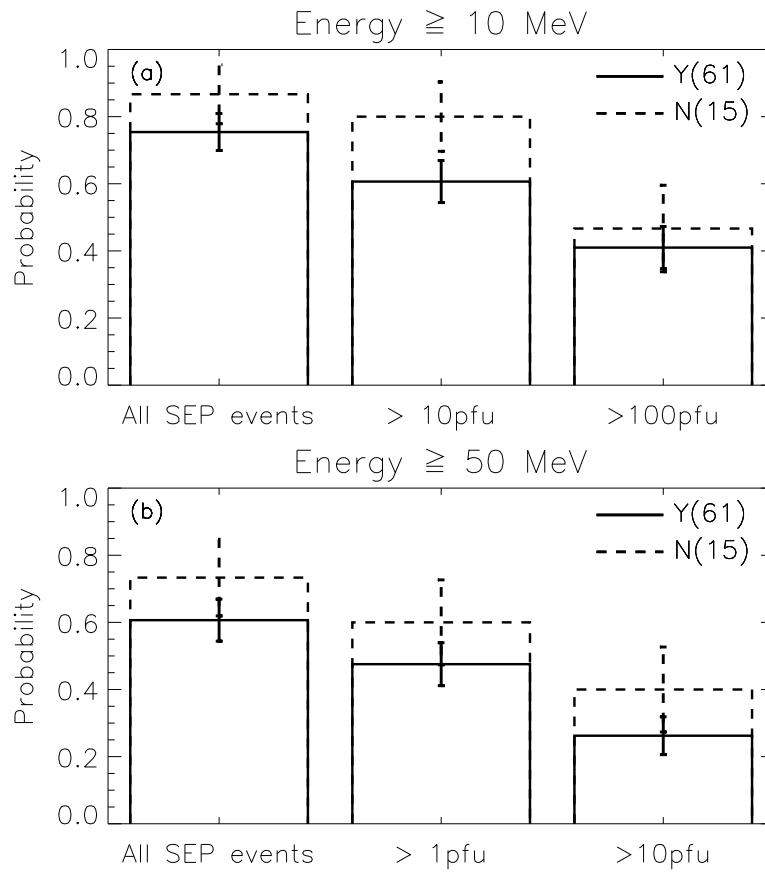


Fig. 6 Occurrence probabilities, P , of SEP events in terms of relative position between CHs and CMEs for proton energies ≥ 10 MeV and ≥ 50 MeV, respectively,

(NCET-08-0524) and the Chinese Academy of Sciences (KZCX2-YW-QN511, KJCX2-YW-N28 and the startup fund).

References

- Altschuler, M. D., & Newkirk. 1969, *Sol. Phys.*, 9, 131
 DeForest, C. E., Lamy, P. L., & Llebaria, A. 2001, *Astrophys. J.*, 560, 490
 Ebert, R. W. , McComas, D. J., Elliott, H. A. ,Forsyth, R. J. & Gosling, J. T., 2009, *J. Geophys. Res.*, 114, A01109
 Fisher, R., & Guhathakurta, M. 1995, *Astrophys. J.*, 447, L139
 Gopalswamy, N., Yashiro, S., Akiyama, S., Makela, P., Xie, H., Kaiser, M. L., Howard, R. A., & Bougeret, J. L. 2008, *Ann. Geophys.*, 26, 3033
 Harvey, K. L., & Recely, F. 2002, *Sol. Phys.*, 211, 31
 Kahler, S. W. 2004, *Astrophys. J.*, 603, 330
 Kunches, J. M., & Zwickl, R. D. 1999, *Radiation Measurements*, 30, 281
 Munro, R. H., & Jackson, B. V. 1977, *Astrophys. J.*, 213, 874
 Reames, D.V. 1999, *Space Sci. Rev.* 90, 413

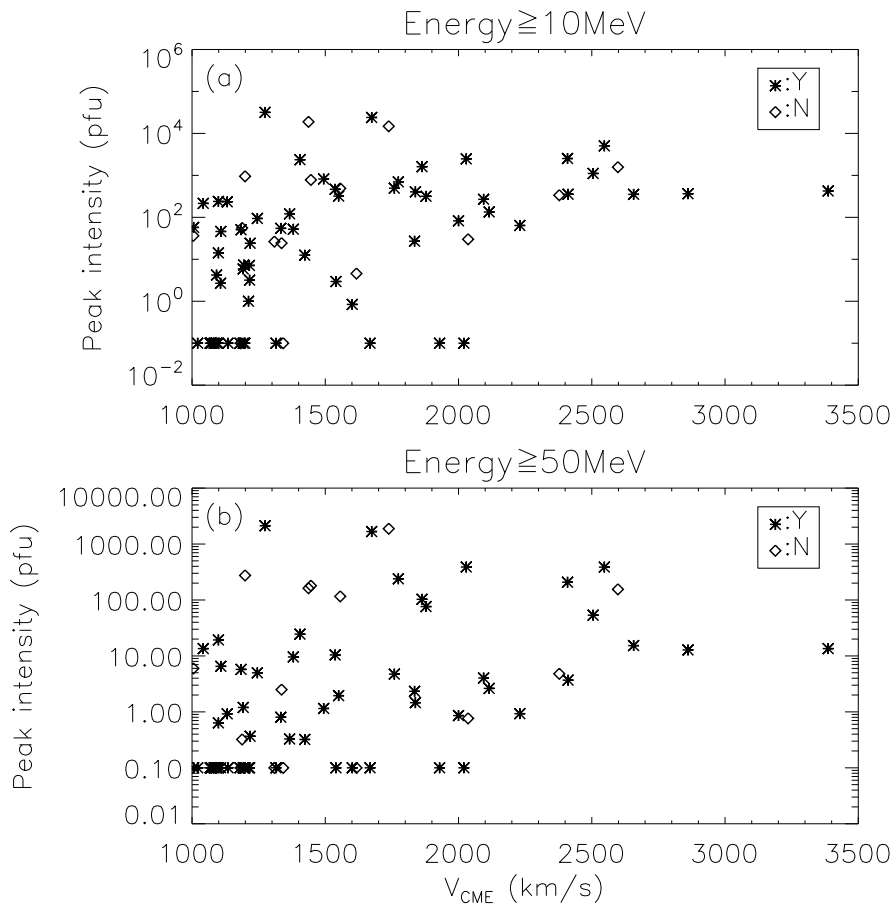


Fig. 7 The peak intensity of proton with energy ≥ 10 MeV vs. associated CME speed. The asterisks show the CMEs in group 'Y' while diamonds show the CME in group 'N'.

Schatten, K. H. 1971, *Cosmic Eledrodyn.*, 2, 232

Schatten, K. H., W., W. J., & F., N. N. 1969, *Sol. Phys.*, 6, 442

Scherrer, P. H., Bogart, R. S., Bush, R. I., Hoeksema, J. T., Kosovichev, A. G., Schou, J., Rosenberg, W., Springer, L., Tarbell, T. D., Title, A., Wolfson, C. J., Zayer, I., & MDI Engineering Team. 1995, *Sol. Phys.*, 162, 129

Shen, C., Wang, Y., Ye, P., Zhao, X. P., Gui, B., & Wang, S. 2007, *Astrophys. J.*, 670, 849

Shen, C. l., Wang, Y. M., Ye, P. Z., & Wang, S. 2006, *Astrophys. J.*, 639, 510

Shen, C. l., Wang, Y. M., Ye, P. Z., & Wang, S. 20068, *Sol. Phys.*, 252, 409

Zhao, X. P., & Hoeksema, J. T. 1992, *Eur. Space Agency Spec. Publ.*, ESA SP-348, 117

—. 1994, *Sol. Phys.*, 151, 91

—. 1995, *J. Geophys. Res.*, 100, 19

Zhao, X. P., Hoeksema, J. T., & Rich, N. B. 2002, *Adv. Space Res.*, 29, 411

Zirker, J. B. 1977, *Reviews of Geophysics and Space Physics*, 15, 257

Table 1 Frontside fast halo CMEs originating from the west hemisphere during 1997 – 2008

No.	Date Time	CME ^a			CH			SEP	
		Width	Speed	Location ^b	Proximity ^c	Area ^d	P ^e	≥10MeV ^f	≥50MeV ^g
1	1997-11-06, 12:10:41	360	1556	S18,W62	0.60(D)	0.0049(a)	N	490.0	116.0
2	1998-04-20, 10:07:11	165	1863	S47,W70	0.28(d)	0.0041(a)	Y	1610.0	103.0
3	1998-05-06, 08:29:13	190	1099	S15,W68	0.54(D)	0.0066(A)	Y	239.0	19.3
4	1999-06-04, 07:26:54	150	2230	N19,W85	0.86(D)	0.0053(a)	Y	64.0	0.9
5	1999-06-28, 21:30:00	360	1083	N23,W42	0.51(D)	0.0070(A)	Y	-1.0	-1.0
6	1999-09-16, 16:54:00	147	1021	N42,W30	0.31(d)	0.0045(a)	Y	-1.0	-1.0
7	2000-02-12, 04:31:00	360	1107	N13,W28	0.51(D)	0.0116(A)	Y	2.7	-1.0
8	2000-04-04, 16:32:00	360	1188	N16,W60	0.07(d)	0.0034(a)	N	55.8	0.3
9	2000-05-15, 16:26:00	>165	1212	S23,W68	0.87(D)	0.0028(a)	Y	1.0	-1.0
10	2000-06-10, 17:08:00	360	1108	N22,W40	0.25(d)	0.0059(a)	Y	46.0	6.5
11	2000-06-25, 07:54:00	165	1617	N10,W60	0.31(d)	0.0066(A)	N	4.6	-1.0
12	2000-06-28, 19:31:00	>134	1198	N24,W85	0.05(d)	0.0119(A)	Y	-1.0	-1.0
13	2000-07-14, 10:54:00	360	1674	N17,W 2	0.97(D)	0.0101(A)	Y	24000.0	1670.0
14	2000-09-12, 11:54:00	360	1550	S14, W 6	0.69(D)	0.0037(a)	Y	321.0	2.0
15	2000-09-16, 05:18:00	360	1215	N13, W 6	0.11(d)	0.0296(A)	Y	7.1	-1.0
16	2000-11-08, 23:06:00	>170	1738	N14,W64	0.88(D)	0.0045(a)	N	14800.0	1880.0
17	2000-11-24, 15:30:00	360	1245	N21,W12	0.30(d)	0.0025(a)	Y	94.0	5.0
18	2001-02-11, 01:31:00	360	1183	N21,W60	0.19(d)	0.0056(a)	N	-1.0	-1.0
19	2001-04-02, 22:06:00	244	2505	N16,W65	0.54(D)	0.0103(A)	Y	1110.0	53.5
20	2001-04-09, 15:54:00	360	1192	S20, W 4	1.06(D)	0.0081(A)	Y	5.9	1.2
21	2001-04-10, 05:30:00	360	2411	S20,W10	1.07(D)	0.0065(A)	Y	355.0	3.7
22	2001-04-12, 10:31:00	360	1184	S20,W43	1.00(D)	0.0102(A)	Y	50.5	5.8
23	2001-04-15, 14:06:00	167	1199	S20,W85	1.03(D)	0.0111(A)	N	951.0	275.0
24	2001-04-26, 12:30:00	360	1006	N23,W 2	0.83(D)	0.0128(A)	Y	57.5	-1.0
25	2001-07-19, 10:30:00	166	1668	S 9,W61	0.36(D)	0.0033(a)	Y	-1.0	-1.0
26	2001-10-01, 05:30:00	360	1405	S20,W89	0.25(d)	0.0054(a)	Y	2360.0	24.5
27	2001-10-22, 15:06:00	360	1336	S18,W20	1.02(D)	0.0081(A)	N	24.2	2.5
28	2001-10-25, 15:26:00	360	1092	S18,W20	0.32(D)	0.0049(a)	Y	-1.0	-1.0
29	2001-11-04, 16:20:00	360	1274	N 6,W18	0.58(D)	0.0036(a)	Y	31700.0	2120.0
30	2001-11-22, 23:30:00	360	1437	S17,W35	0.14(d)	0.0046(a)	N	18900.0	162.0
31	2001-12-26, 05:30:00	>212	1446	N 9,W61	0.27(d)	0.0047(a)	N	780.0	180.0
32	2002-04-17, 08:26:00	360	1218	N13,W12	0.22(d)	0.0068(A)	Y	24.1	0.4
33	2002-04-21, 01:27:00	241	2409	S18,W79	0.06(d)	0.0081(A)	Y	2520.0	208.0
34	2002-05-22, 03:50:00	360	1494	S15,W70	0.73(D)	0.0065(A)	Y	820.0	1.1
35	2002-07-15, 20:30:00	360	1132	N20,W 2	0.08(d)	0.0164(A)	Y	234.0	0.9
36	2002-07-18, 08:06:00	360	1099	N20,W33	0.05(d)	0.0098(A)	Y	14.2	0.6
37	2002-08-06, 18:25:00	134	1098	S38,W18	0.31(d)	0.0040(a)	Y	-1.0	-1.0
38	2002-08-14, 02:30:00	133	1309	N10,W60	0.04(d)	0.0083(A)	N	26.4	-1.0
39	2002-08-22, 02:06:00	360	1005	S14,W60	0.46(D)	0.0035(A)	N	36.4	6.0
40	2002-08-24, 01:27:00	360	1878	S 5,W89	0.28(d)	0.0041(a)	Y	317.0	76.2
41	2002-11-09, 13:31:00	360	1838	S 9,W30	0.42(D)	0.0105(A)	Y	404.0	1.5
42	2002-12-19, 22:06:00	360	1092	N16,W10	0.58(D)	0.0170(A)	Y	4.2	-1.0
43	2002-12-21, 02:30:00	225	1072	N30,W 0	0.75(D)	0.0190(A)	Y	-1.0	-1.0
44	2002-12-22, 03:30:00	272	1071	N24,W43	0.69(D)	0.0224(A)	Y	-1.0	-1.0
45	2003-03-18, 12:30:00	209	1601	S13,W48	0.14(d)	0.0199(A)	Y	0.8	-1.0
46	2003-03-19, 02:30:00	360	1342	S13,W56	0.17(d)	0.0212(A)	N	-1.0	-1.0
47	2003-05-28, 00:50:00	360	1366	S 5,W25	0.12(d)	0.0044(a)	Y	121.0	0.3
48	2003-05-31, 02:30:00	360	1835	S 5,W65	0.18(d)	0.0034(a)	Y	27.0	2.3
49	2003-10-26, 17:54:00	>171	1537	N 3,W43	0.15(d)	0.0032(a)	Y	466.0	10.4
50	2003-10-27, 08:30:00	>215	1380	N 3,W48	0.08(d)	0.0028(a)	Y	52.0	9.6
51	2003-10-29, 20:54:00	360	2029	S16,W 5	0.72(D)	0.0027(A)	Y	2470.0	389.0
52	2003-11-02, 09:30:00	360	2036	S16,W51	0.07(d)	0.0035(a)	N	30.0	0.8
53	2003-11-02, 17:30:00	360	2598	S16,W56	0.08(d)	0.0035(a)	N	1570.0	155.0
54	2003-11-04, 19:54:00	360	2657	S16,W83	0.07(d)	0.0037(a)	Y	353.0	15.3
55	2003-11-11, 13:54:00	360	1315	S 3,W63	0.24(d)	0.0049(a)	Y	-1.0	-1.0
56	2004-04-08, 10:30:19	360	1068	S16,W 6	0.02(d)	0.0033(a)	Y	-1.0	-1.0
57	2004-07-25, 14:54:05	360	1333	N 3,W33	0.72(D)	0.0028(a)	Y	54.6	0.8
58	2004-07-29, 12:06:05	360	1180	N 0,W89	0.32(D)	0.0060(a)	Y	-1.0	-1.0
59	2004-07-31, 05:54:05	197	1192	N 9,W89	0.37(D)	0.0059(a)	Y	-1.0	-1.0
60	2004-11-07, 16:54:05	360	1759	N 9,W16	0.38(D)	0.0220(A)	Y	495.0	4.7
61	2004-11-09, 17:26:06	360	2000	N 8,W48	0.31(d)	0.0270(A)	Y	82.4	0.9
62	2004-11-10, 02:26:05	360	3387	N 7,W53	0.12(d)	0.0259(A)	Y	424.0	13.5
63	2004-12-03, 00:26:05	360	1216	N 9,W 1	0.35(D)	0.0028(a)	Y	3.2	-1.0
64	2005-01-15, 23:06:50	360	2861	N13,W 3	0.76(D)	0.0112(A)	Y	365.0	12.8
65	2005-01-17, 09:30:05	360	2094	N13,W20	0.46(D)	0.0245(A)	Y	269.0	4.0
66	2005-01-17, 09:54:05	360	2547	N13,W20	0.46(D)	0.0245(A)	Y	5040.0	387.0
67	2005-01-19, 08:29:39	360	2020	N13,W45	0.51(D)	0.0246(A)	Y	-1.0	-1.0
68	2005-02-17, 00:06:05	360	1135	S 1,W19	0.02(d)	0.0059(a)	Y	-1.0	-1.0
69	2005-07-09, 22:30:05	360	1540	N 9,W29	0.31(d)	0.0313(A)	Y	3.0	-1.0
70	2005-07-13, 14:30:05	360	1423	N 9,W76	0.33(D)	0.0382(A)	Y	12.5	0.3
71	2005-07-14, 10:54:05	360	2115	N 9,W87	0.39(D)	0.0395(A)	Y	134.0	2.6
72	2005-08-22, 01:31:48	360	1194	S12,W51	0.18(d)	0.0027(a)	Y	7.3	-1.0
73	2005-08-22, 17:30:05	360	2378	S12,W60	0.18(d)	0.0027(a)	N	337.0	4.8
74	2005-08-23, 14:54:05	360	1929	S13,W75	0.24(d)	0.0035(a)	Y	-1.0	-1.0
75	2006-12-13, 02:54:04	360	1774	S 8,W19	0.14(d)	0.0027(a)	Y	698.0	239.0
76	2006-12-14, 22:30:04	360	1042	S10,W42	0.19(d)	0.0032(a)	Y	215.0	13.5

^a Obtained from CME CATALOG (<http://cdaw.gsfc.nasa.gov/CME-list/>).^b CME locations determined by the EIT movie.^c Shortest surface distance between a CME and a CH (from the CME site to the CH boundary) in units of R_{\odot} , called CH-proximity. 'D' means CH proximity larger than0.3 R_{\odot} while 'd' means others.^d Area of the closest CH in units of A_{\odot} the area of solar surface. 'A' means the CH area larger than 0.0061 A_{\odot} while 'a' means it smaller than 0.0061 A_{\odot} .

Table 2 Mean value of CME speed for different groups (in unit of $km.s^{-1}$)

Energy	SEP	CH Proximity		CH area		Relative Position	
		d	D	a	A	Y	N
≥ 10 MeV	Y	1663 ± 560^a	1623 ± 524	1604 ± 454	1682 ± 614	1655 ± 559	1603 ± 474
	N	1254 ± 274	1297 ± 353	1262 ± 282	1298 ± 369	1276 ± 324	1263 ± 112
≥ 50 MeV	Y	1726 ± 605	1727 ± 518	1650 ± 459	1817 ± 655	1755 ± 574	1629 ± 511
	N	1318 ± 251	1232 ± 288	1250 ± 249	1305 ± 292	1264 ± 280	1363 ± 183

^a The number after \pm shows the standard variation.